Supplementary Information

Fabrication of $CoSe_2/FeSe_2$ heterostructures with stable solid electrolyte interface film and low surface activation energy for Na-ion batteries

Zhiya Lin [a,c], Zhilong Wu [b], Maoxin Yu [b], Hai Jia [a], Kaiqiang Zhou [d], Xiaohui Huang [b*] and Shaoming Ying [b*]

[a] College of Mathematics and Physics, Ningde Normal University, Ningde, 352100, China.

[b] College of New Energy and Materials, Ningde Normal University, Fujian Provincial Key Laboratory of Featured Materials in Biochemical Industry, Ningde 352100, China.

[c] College of Physics and Energy, Fujian Normal University, Fujian Provincial Solar Energy Conversion and Energy Storage Engineering Technology Research Center, Fuzhou, 350117, China.

[d] School of Physics and Information Engineering, Minnan Normal University, Zhangzhou, 363000, China.

*Corresponding author:

Xiaohui Huang E-mail: 11429721@qq.com

Shaoming Ying E-mail: yingshaoming@126.com

1. Experimental

1.1 Synthesis of FeCo-PBA precursor

The cubic FeCo-PBA precursor were prepared by coprecipitation method. 4 mmol $K_3[Fe(CN)_6]$ were dissolved in 200 ml DI water to form solution A. In a separate container, dissolve 6 mmol of $Co(NO_3)_2 \cdot 6H_2O$ and 9 mmol of $C_6H_5Na_3O_7$ in 200 ml of deionized water to prepare solution B. Slowly pour solution A into solution B while stirring for 10 minutes, then allow the mixture to stand undisturbed for 24 hours. After centrifugation and drying, the resulting purplish-red sample is the cobalt-iron Prussian blue compound (CoFe-PBA).

1.2 Synthesis of FeCo-PBA@PDA composites

100 mg cubic FeCo-PBA were first dispersed into 100 mL tris-buffer solution (PH=8.5) by ultrasonication for 15 min. Then, 60 mg of dopamine hydrochloride was added into the above solution, which was kept stirring for 12 h. The resultant product hexagon FeCo-PBA@PDA was collected through centrifugation and washed several times with absolute ethyl alcohol and deionized water, respectively, and dried at 70 °C overnight.

1.3 Synthesis of $CoSe_2/FeSe_2$ and YS- $CoSe_2/FeSe_2$@NC composites

The as-prepared FeCo-PBA or FeCo-PBA@PDA precursors and Se powders with a weight ratio of (1:4) were put in a corundum boat and calcined at 450 °C in Ar atmosphere for 2.5 h. Then the $CoSe_2/FeSe_2$ and YS-$CoSe_2/FeSe_2$@NC composites were obtained.

1.4 Materials characterization

The crystalline phase and morphology of the as-prepared FeCo-PBA, $CoSe_2/FeSe_2$ and YS-$CoSe_2/FeSe_2$@NC composites was investigated by powder X-ray diffractometry (XRD, BRUKER D8 ADVANCE) with Cu-Kα radiation

(λ=0.15406 nm) and scanning electron microscopy (SEM, SU8010). The microstructure of $CoSe_2/FeSe_2$ and YS-$CoSe_2/FeSe_2$@NC composites are further identified by transmission electron microscopy (TEM, TJEOL JEM 2100). The specific surface area and pore volume of the samples were analyzed by Brunauer Emmett-Teller (BET) measurements using a TriStar II 3020 surface area analyzer. The chemical composition and valence states of YS-$CoSe_2/FeSe_2$@NC is analysed by X-ray photoelectron spectroscope (XPS ESCALAB 250Xi, Thermo Scientific).

1.5 Cell fabrication and characterization

The sodium storage performance of $CoSe_2/FeSe_2$ and YS-$CoSe_2/FeSe_2$@NC are evaluated with CR2025-type coin cells. The $CoSe_2/FeSe_2$ and YS-$CoSe_2/FeSe_2$@NC are combined with Super-P (SP) and polyvinylidene fluoride (PVDF) binder in a mass ratio of 7:2:1 in N-methylpyrrolidone (NMP) to create a homogeneous slurry. This slurry is then cast onto copper foil and dried in a vacuum at 110 °C for 12 hours. After drying, electrode discs with a diameter of 12.5 mm are punched out and weighed, resulting in an active material loading density of approximately 1.4 mg/cm^2. Electrochemical cells are assembled in an argon-filled glove box where the levels of O_2 and H_2O are maintained below 0.01 ppm. The electrolyte used is 1 M $NaPF_6$ in diethylene glycol dimethyl ether (DEGDME), with sodium foil serving as both the anode and counter electrode. A Whatman glass microfiber filter (Whatman GF/F) is employed as the separator. Galvanostatic charge/discharge measurements are conducted within a voltage range of 0.01 to 3.0 V using a multichannel battery testing system (LAND CT2001A). Cyclic voltammetry (CV) and electrochemical impedance spectroscopy (EIS) for the prepared anodes are performed using an electrochemical workstation (Metrohm Autolab PGSTAT302N) with a voltage window of 0.01 to 3.0 V. Galvanostatic intermittent titration technique (GITT) measurements were carried

out by applying a constant current of 50 mA g^{-1} for 300 s followed by a 900 s relaxation to reach equilibrium.

1.6 Computational Method

Density Functional Theory (DFT) calculations were carried out within the framework of the generalized gradient approximation (GGA), utilizing the Perdew-Burke-Ernzerhof (PBE) functional [1], as implemented in the Vienna Ab Initio Simulation Package (VASP 6.1.2) [2,3]. The interactions between ion cores and valence electrons were treated using the projector augmented-wave (PAW) method [4,5]. A plane-wave cutoff energy of 450 eV was employed to ensure the accuracy of the calculations. Van der Waals interactions were included using Grimme's DFT-D3 method [6,7], which provides a reliable description of dispersion forces. Self-consistent calculations were performed with a convergence threshold of 10^{-5} eV, ensuring high precision.

The equilibrium geometries and lattice constants were optimized with a maximum force tolerance of 0.02 eV $Å^{-1}$, and the Brillouin zone was sampled with a 1×1×1 Gamma-centered grid during structural relaxation. To avoid spurious interactions between periodic images, a vacuum layer of 15 Å was incorporated in the surface calculations. Spin-polarized calculations were also carried out to account for magnetic effects in the system.

The adsorption energy (E_{ads}) was computed using the following expression:

$$E_{ads} = E(total) - E(slab) – E(Na)$$

where E(total) represents the total energy of the optimized slab with Na adsorbed, E(slab) is the energy of the relaxed clean slab, and E(Na) denotes the energy of an isolated Na atom in the gas phase.

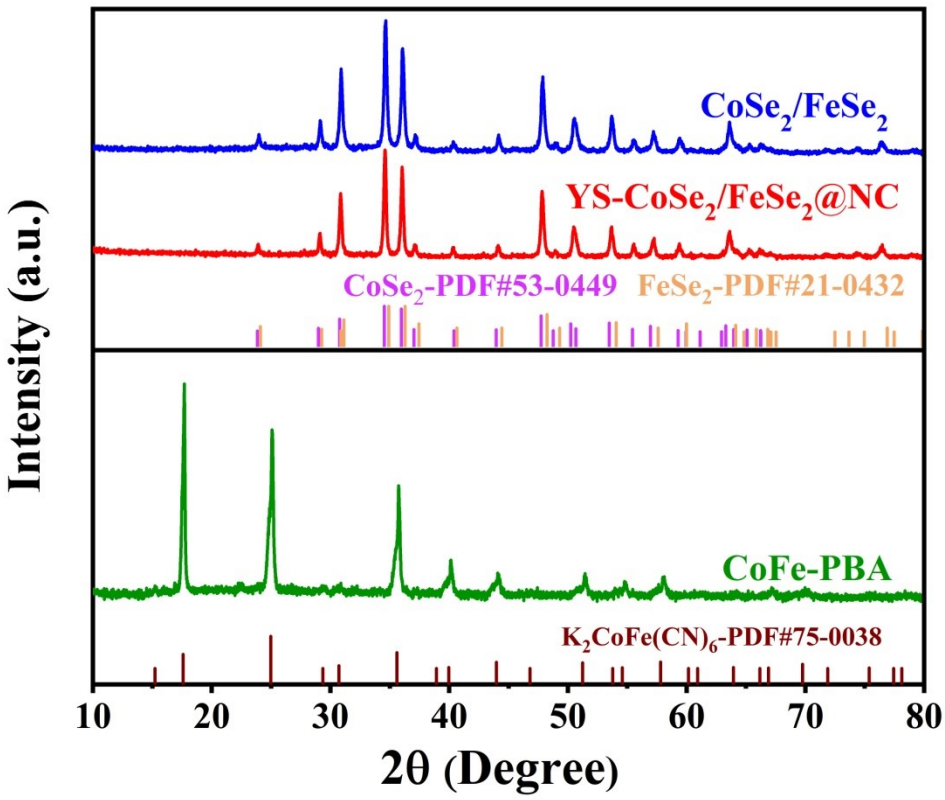

Figure S1 The XRD curves of CoFe-PBA, $CoSe_2/FeSe_2$ and YS-$CoSe_2/FeSe_2$@NC samples.

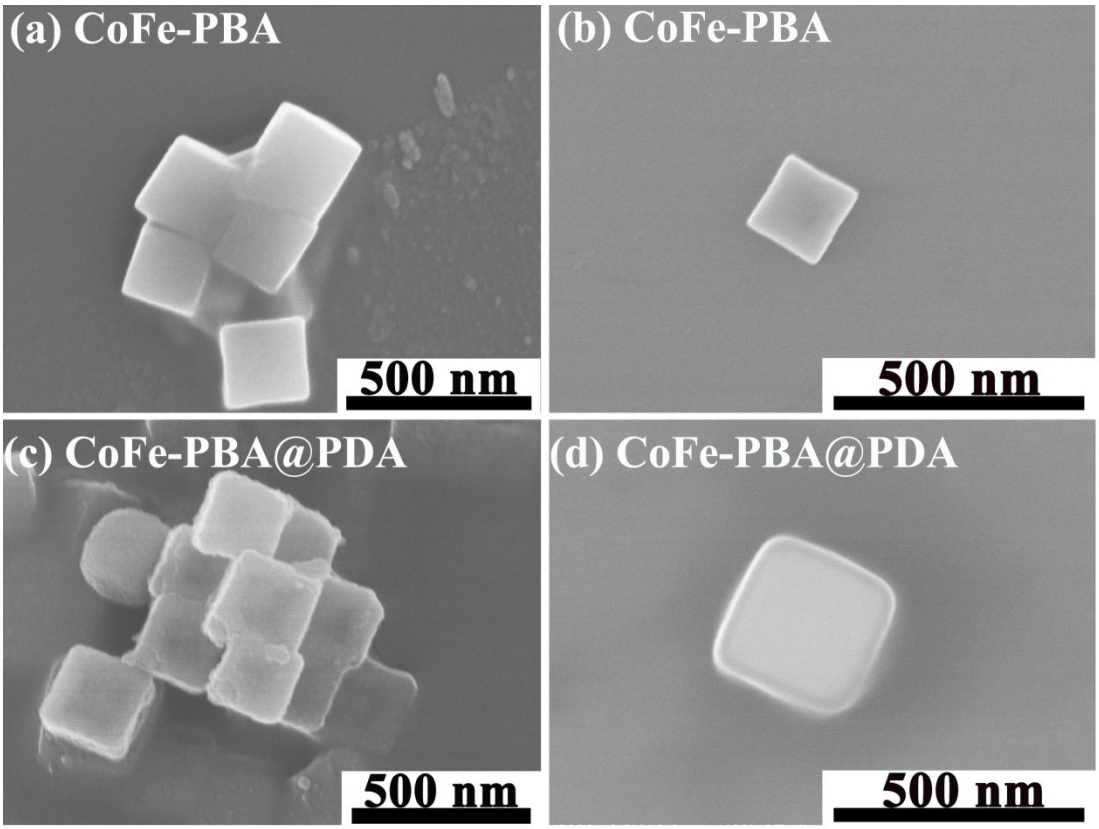

Figure S2 SEM images of (a,b) CoFe-PBA and (c,d) CoFe-PBA@PDA powders.

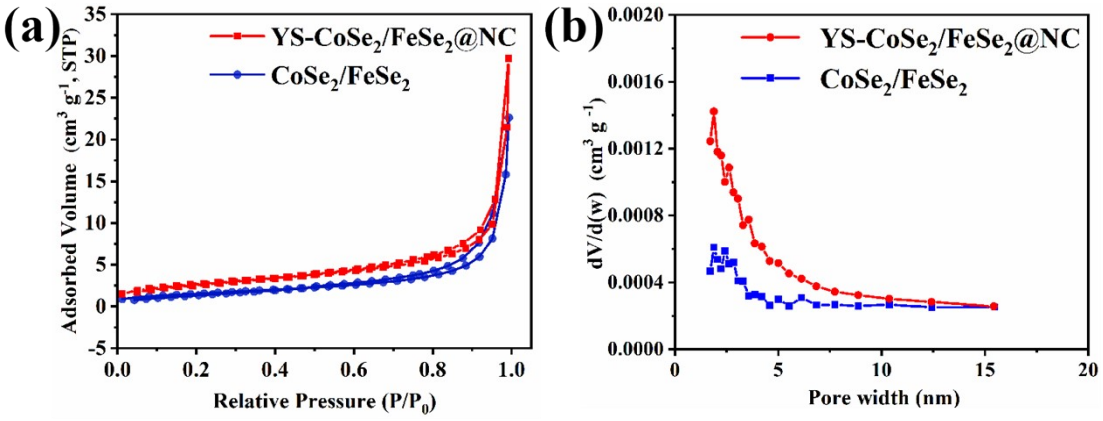

Figure S3 (a) nitrogen sorption isotherms and (b) pore diameter distribution of $CoSe_2/FeSe_2$ and YS-$CoSe_2/FeSe_2$@NC powders.

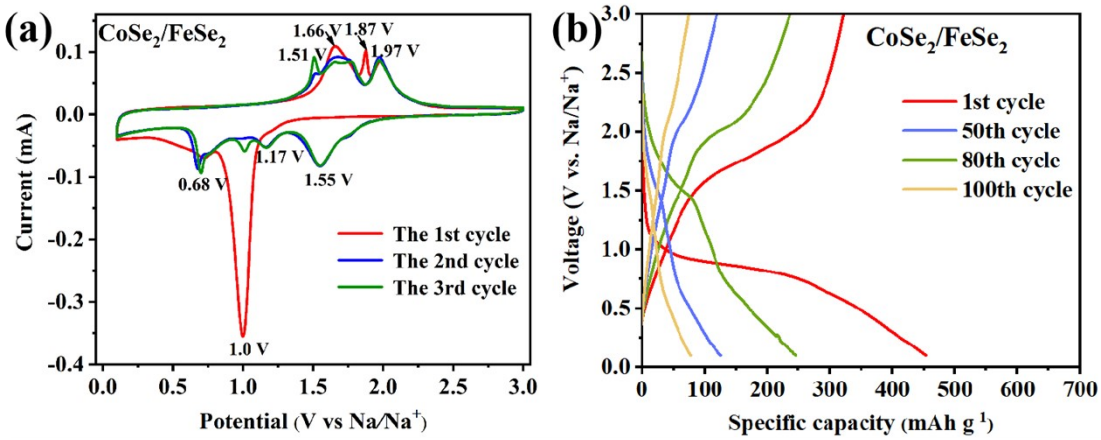

Figure S4 The (a) CV and (b) galvanostatic charge-discharge curves of $CoSe_2/FeSe_2$.

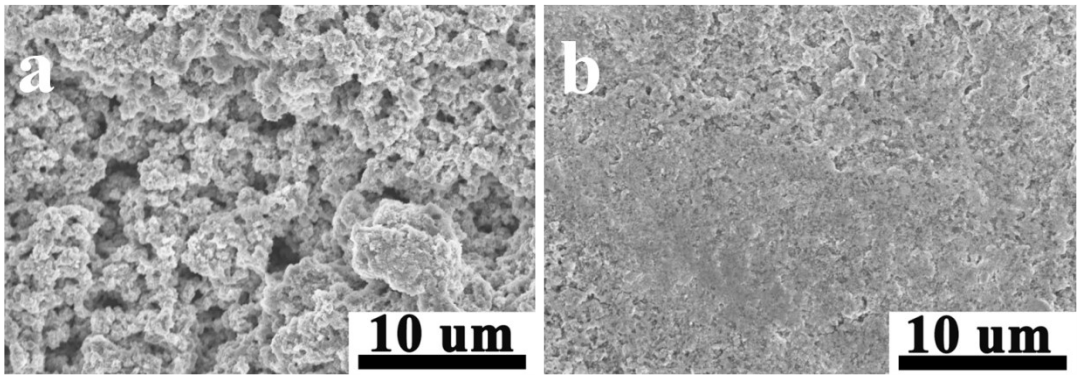

Figure S5 The surface morphologies of (a) $CoSe_2/FeSe_2$ and (b) YS-$CoSe_2/FeSe_2$@NC electrodes after 100 cycles.

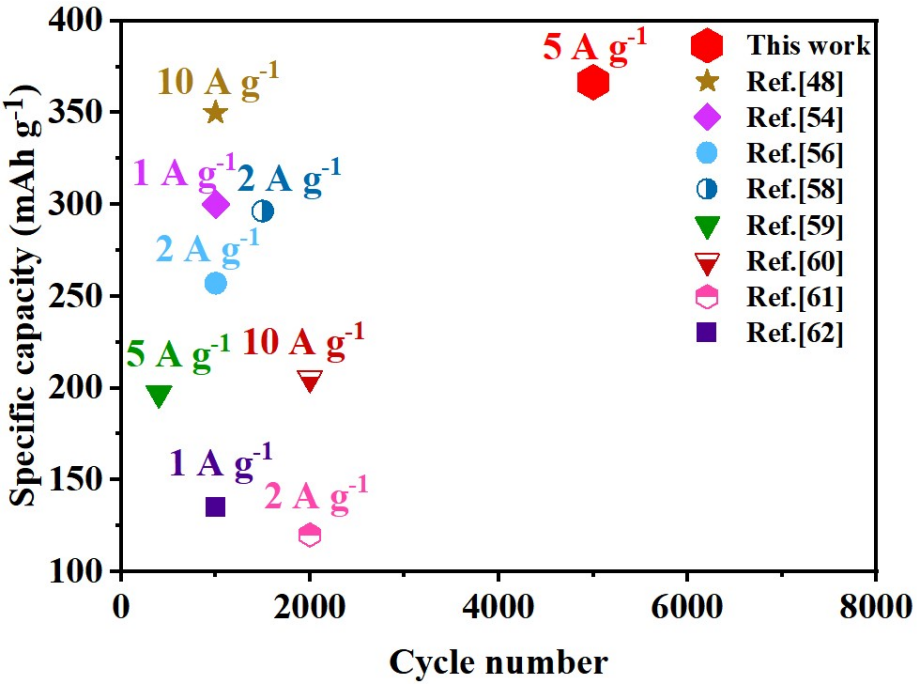

Figure S6 comparison of the cycling capability of the YS- $CoSe_2/FeSe_2$@NC electrode with those of the other heterojunction material.

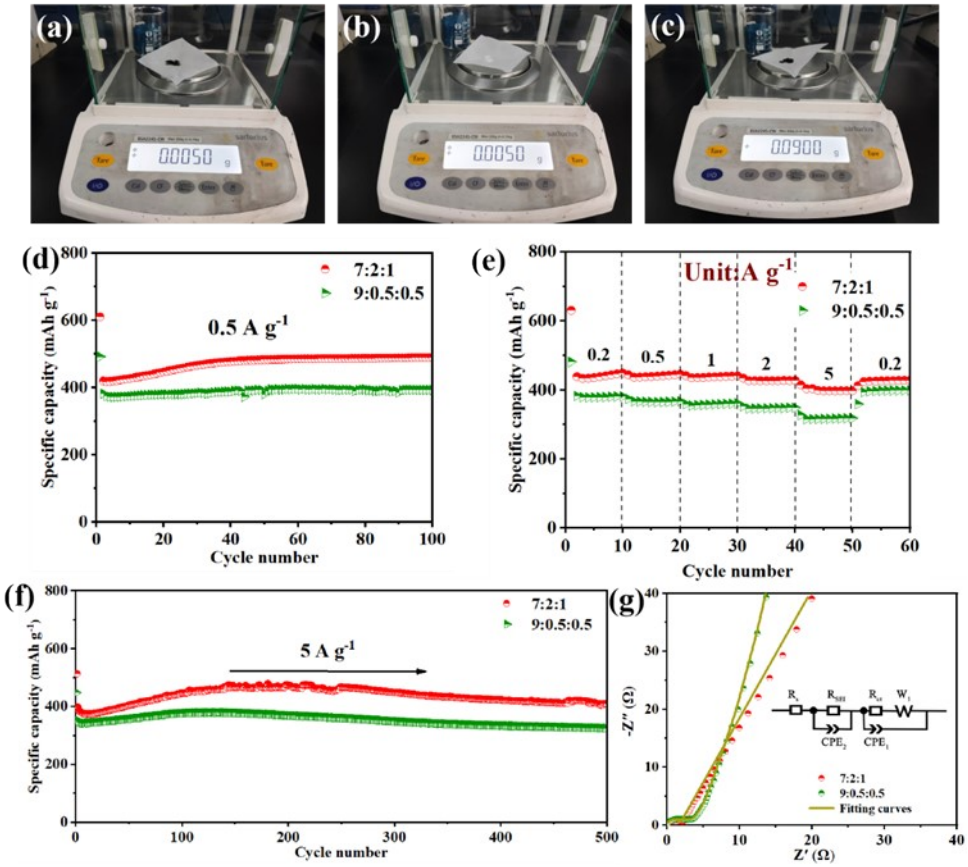

Fig. S7 (a-c) Record of weighing YS-$CoSe_2$/$FeSe_2$@NC with Super-P (SP) and polyvinylidene difluoride (PVDF), (d) Cycle performance of 7:2:1 and 9:0.5:0.5 mass ratios electrodes at current density of 0.5 A g^{-1}, (e) Rate performance of 7:2:1 and 9:0.5:0.5 mass ratios electrodes at various current density, (f) Long-term cyclic capability of 7:2:1 and 9:0.5:0.5 mass ratios electrodes at 5 A g^{-1}. (f) AC impedance spectra of 7:2:1 and 9:0.5:0.5 mass ratios electrodes.

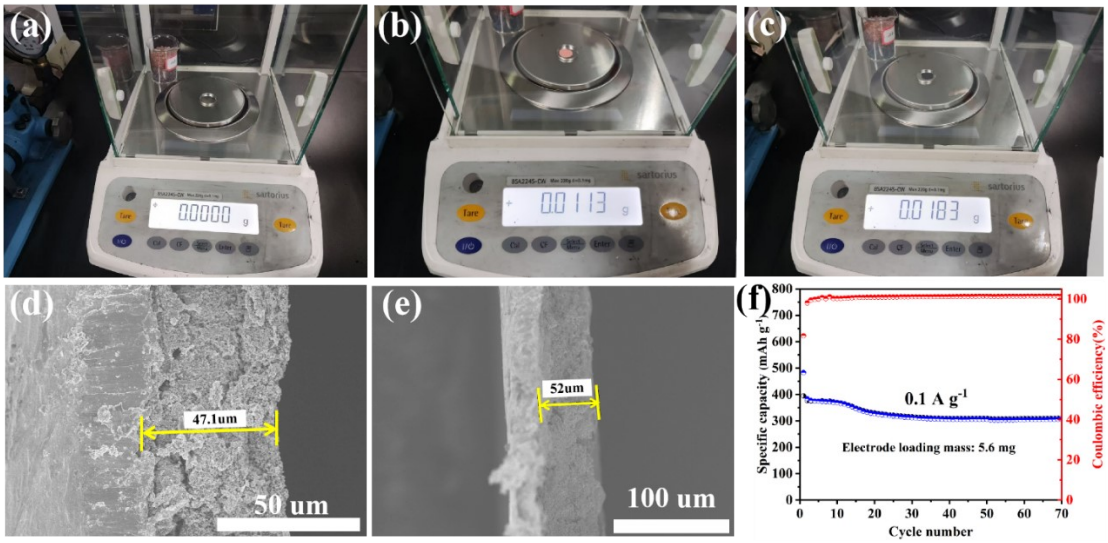

Fig. S8 (a-c) Record of the process of weighing the electrode discs, (d,e) SEM image of the thickness of electrode discs coating, (f) Cycle performance of YS-$CoSe_2$/$FeSe_2$@NC electrodes at current density of 0.1 A g^{-1}.

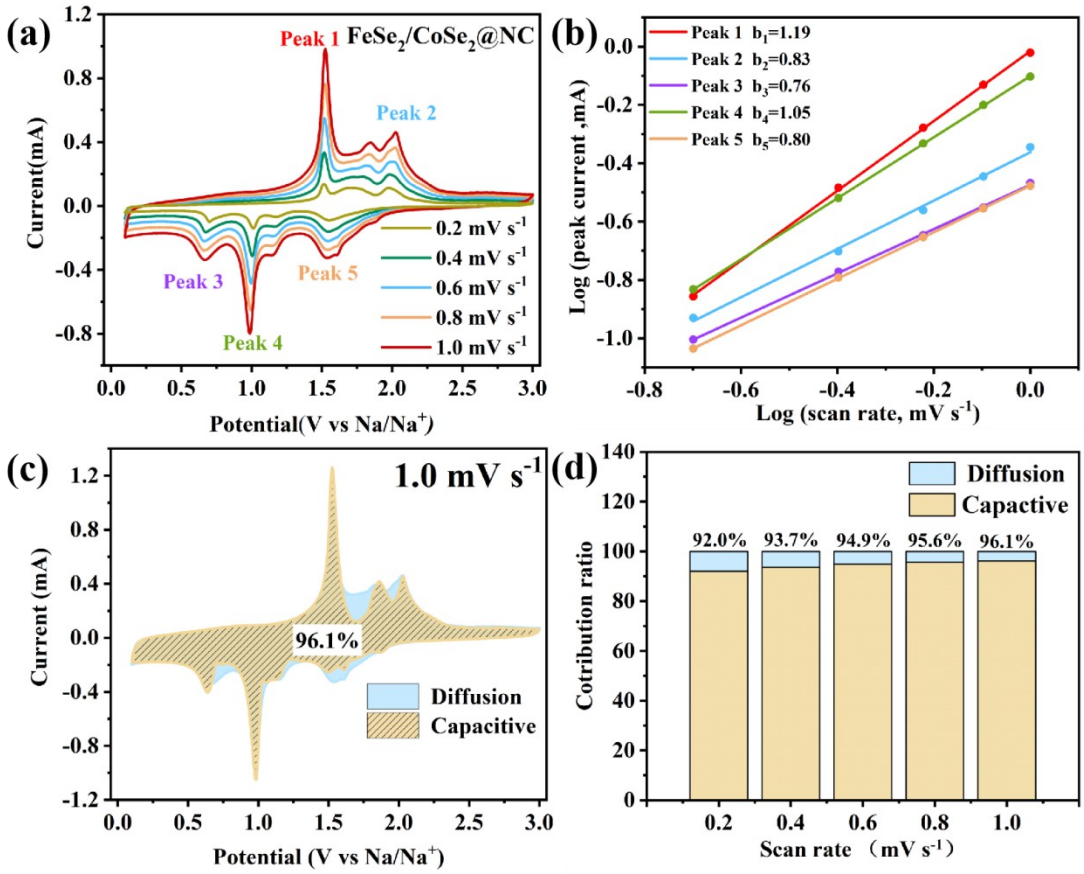

Figure S9 (a) CV curves of the YS-$CoSe_2$/$FeSe_2$@NC electrode in Na coin-cell at various scan rates from 0.1 to 1 mV s^{-1}; (b) Calculation of b-values by the relationship of the scan rate and peak current; (c) CV curve of the YS-$CoSe_2$/$FeSe_2$@NC electrode at 1.0 mV s^{-1} with separation of capacitive and diffusion currents; (d) Contribution ratio of the capacitive and diffusion controlled capacity at different scan rate.

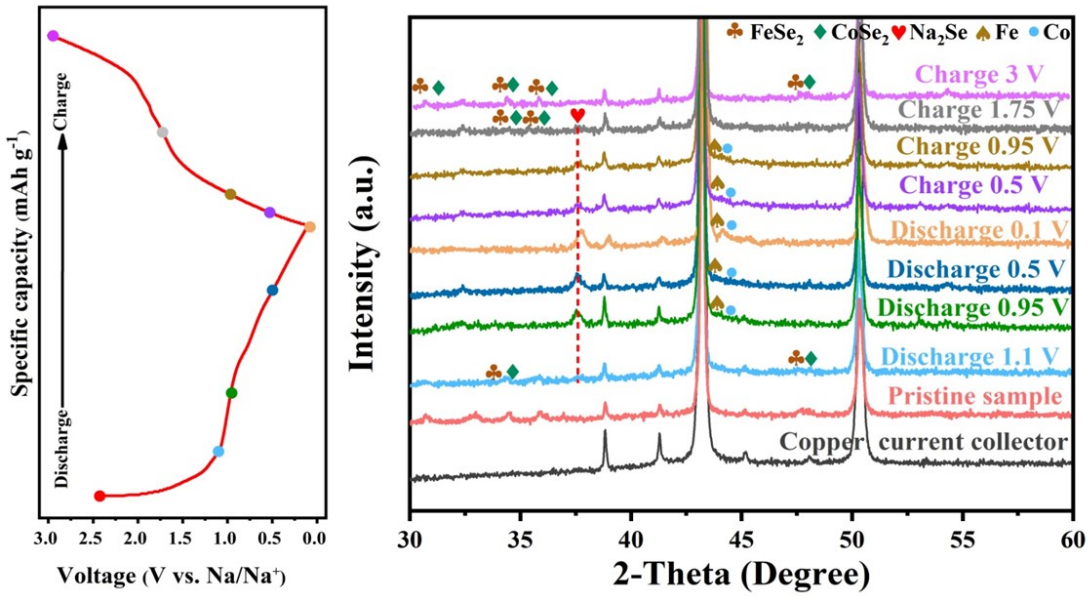

Figure S10 Ex-situ XRD patterns of YS-$CoSe_2$/$FeSe_2$@NC electrode collected during the first electrochemical cycle, with the corresponding charge/discharge profiles in SIBs.

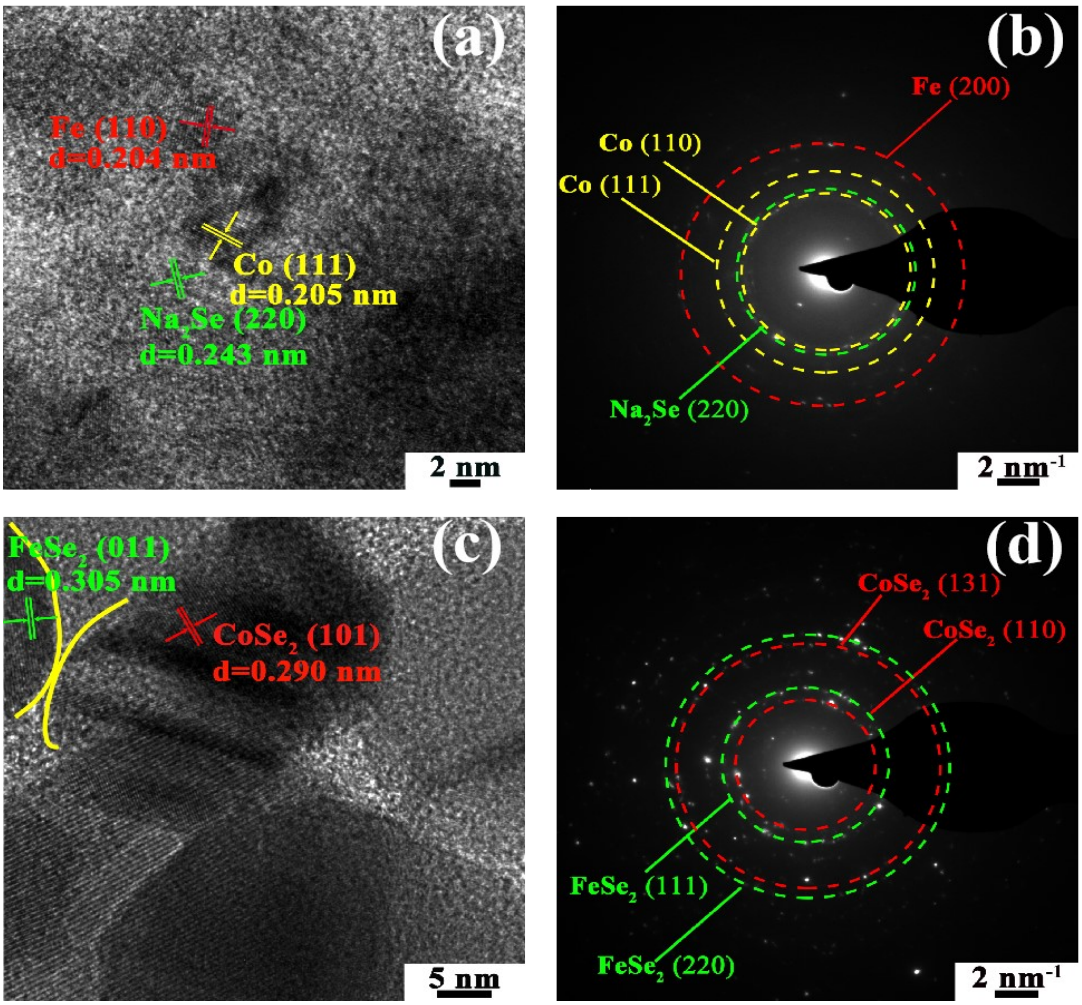

Figure S11 Ex-situ HRTEM and SAED patterns of YS-$CoSe_2$/$FeSe_2$@NC (a,b) after first discharge cycle, (c,d) after first charge cycles.

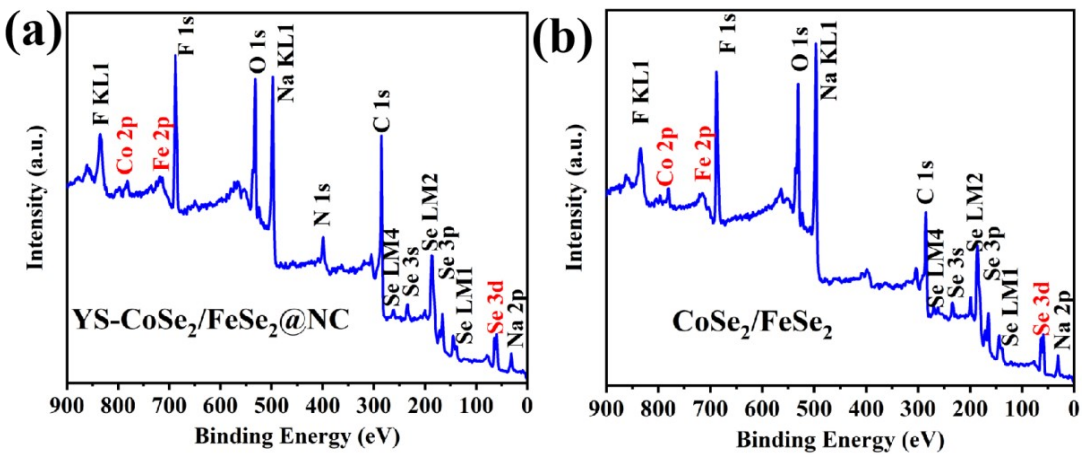

Figure S12 XPS survey spectra of (a) YS-$CoSe_2$/$FeSe_2$@NC and (b) $CoSe_2$/$FeSe_2$ extracted from coin cells after first sodiation/de-sodiation.

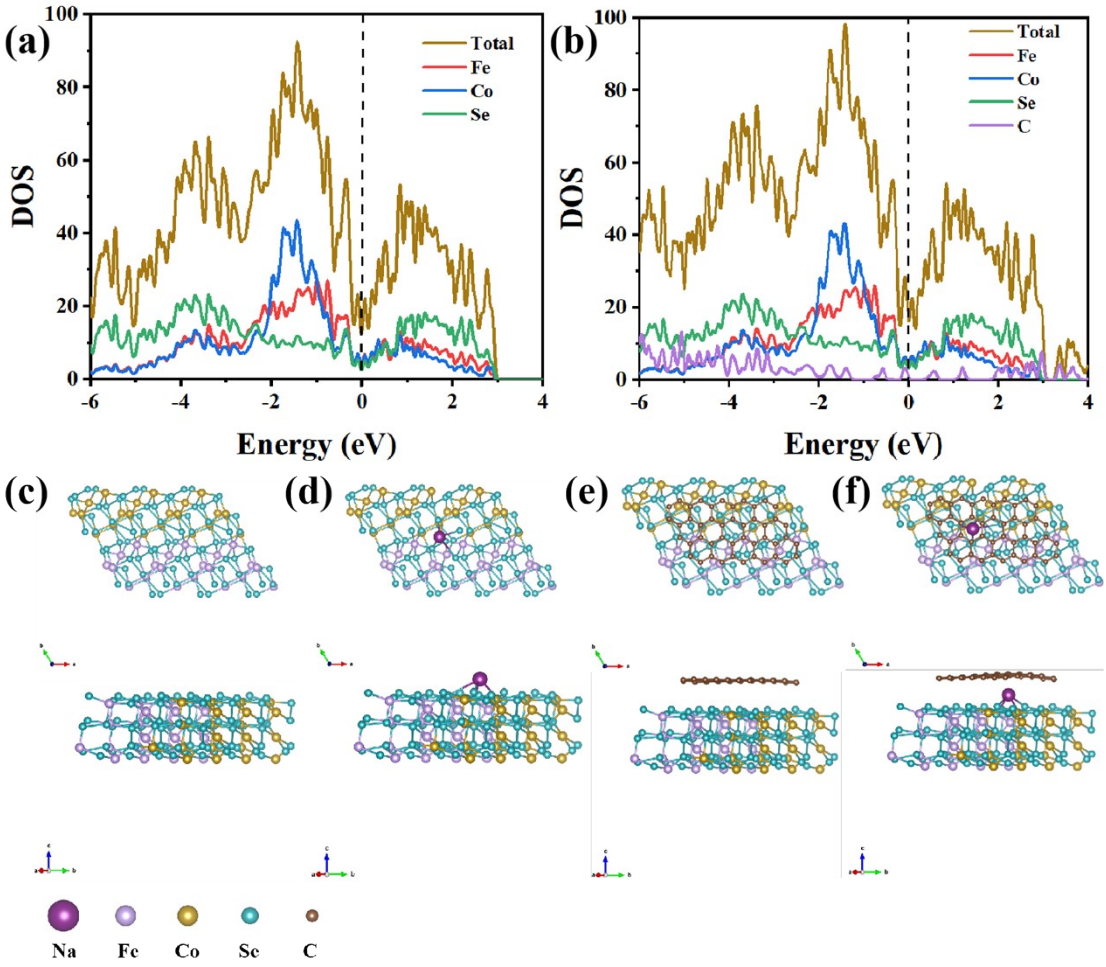

Figure S13 Projected density of states of (a) $CoSe_2/FeSe_2$, and (b) C- $CoSe_2/FeSe_2$, Top view and side view of (c) $CoSe_2/FeSe_2$ (111) and (e) C- $CoSe_2/FeSe_2$ (111) configuration, Na adsorption on (d) $CoSe_2/FeSe_2$ (111) and (f) C- $CoSe_2/FeSe_2$ (111), The spheres with different colors denote C, Se, Co, Fe and Na atoms, respectively.

Table S1. The adsorption energies (E_{ad}) of Na on $CoSe_2/FeSe_2$ (111) and C- $CoSe_2/FeSe_2$ (111).

Compounds	E_{ad}(eV)
$CoSe_2/FeSe_2$	-2.69
C- $CoSe_2/FeSe_2$	-2.75

References

1. J. P. Perdew, K. Burke, M. Ernzerhof, *Phys. Rev. Lett.* 1996, 77, 3865-3868.
2. W. Kohn and L. J. Sham, *Phys. Rev.,* 1965, 140, A1133-A1138.
3. P. Raybaud, J. Hafner, G. Kresse, S. Kasztelan and H. Toulhoat, *J. Catal.,* 2000, 189, 129-146.
4. G.Kresse, D. Joubert, *Phys. Rev. B* 1999, 59, 1758-1775.
5. P. E. Blöchl, *Phys. Rev. B* 1994, 50, 17953-17979.
6. S. Grimme, J. Antony, S. Ehrlich and H. Krieg, *J. Chem. Phys.,* 2010, 132, 154104.
7. S. Grimme, S. Ehrlich and L. Goerigk, *J. Comput. Chem.,* 2011, 32, 1456-1465.